metals

MDPI

Article

The Effect of Soaking Time on Mechanical Properties of Roll-Bonded AA3003 and AA4045 Used for Heat Exchangers

Joseph S. Moema [1,2,*], Charles W. Siyasiya [2], Veronica K. Morudu [1] and Thokozani Buthelezi [3]

[1] Mintek, Advanced Materials Division, Private Bag X3015, Randburg 2125, South Africa; veronicam@mintek.co.za
[2] Department of Material Science & Metallurgical Engineering, The University of Pretoria, Hatfield Campus, Private Bag X20, Pretoria 0028, South Africa; charles.siyasiya@up.ac.za
[3] Hulamin Operations Proprietary Limited, Moses Mabhida Road, Pietermaritzburg 3201, South Africa; thokozani.buthelezi@hulamin.co.za
* Correspondence: josephm@mintek.co.za; Tel.: +27-(0)11-709-4488

Abstract: Due to the rising need for energy saving, high-performing automotive heat exchangers, demand has significantly grown in recent years. As a result, effective fin-tube heat exchangers are becoming more popular. These tubes are typically made by rolling flat strips of AA3003 aluminum alloys that have either one or both sides coated with AA4xxx alloys. The AA3003 type of alloy is typically used as the core, which is then covered in either AA4045 or AA4343, which melts during the brazing process to adhere the fins to the tubes. To maintain the optimal size and distribution of manganese (Mn)-containing precipitates, preheating parameters are carefully controlled. Then, longer soaking times or higher soaking temperatures result in larger precipitates, which cause the final product to exhibit poor mechanical properties. Therefore, it is crucial to optimize the different manufacturing steps, such as homogenization, soaking time, and brazing in order to achieve a high quality product. Studies on the impact of homogenization temperature and time on the microstructure of AA3xxx aluminum alloys have been conducted. However, there has been little research on the impact of soaking (reheating) time on AA3003 cladded alloys. Hence, the effects of isothermal soaking time on the microstructure and mechanical properties of AA3003 cladded with AA4045 alloy were investigated in this work. Optical microscopy (OM) and scanning electron microscopy (SEM) were used to characterize the microstructure and identify intermetallic phases. The final microstructure in terms of grain structure at various homogenization times was characterized by electron backscattered diffraction (EBSD). After the hot-rolling and cold-rolling of the as-received material, large particles of intermetallic (mainly in the form of Chinese script morphology consisting of Fe-Mn-Si) were broken into smaller particles with an increased Fe, Mn, and Si content, indicating the formation of an α-Al(Fe,Mn)Si phase. The α-Al(Mn,Fe)Si was found to be a dominant dispersoid precipitate in the modified AA3003 core. Coarsening of the Al(Mn,Fe)Si dispersoids at 505 °C was only observed at a 45 h homogenization time. The hardness trend with homogenization time was found to be similar to that after homogenization, cold working, and annealing, with exception of an increase in hardness in the latter possibly due to strain hardening (from cold-rolling).

Keywords: thermomechanical process; manufacturing processes; aluminum alloys; microstructures; hardness; AA3003 alloy; AA4045 alloy

Citation: Moema, J.S.; Siyasiya, C.W.; Morudu, V.K.; Buthelezi, T. The Effect of Soaking Time on Mechanical Properties of Roll-Bonded AA3003 and AA4045 Used for Heat Exchangers. *Metals* **2023**, *13*, 1636. https://doi.org/10.3390/met13101636

Academic Editors: Marcello Cabibbo and Zbigniew Pater

Received: 26 June 2023
Revised: 6 September 2023
Accepted: 19 September 2023
Published: 23 September 2023

1. Introduction

AA3XXX series alloys are the most common heat-exchanger tube materials. They are usually roll-plated with a lower-melting silicon-containing AA4XXX series alloy that melts during the brazing process of heat exchanger manufacture and forms the joints between the different parts of the heat exchanger. This alloy is heat-treatable and has very good flow characteristics. This wrought aluminum alloy has Si as the main alloying element in

AA4045 and Mn as a minor alloying element. AA4045 is mainly used as a filler material since it has a melting interval.

Manganese is the main alloying element of the AA3xxx core alloys; it assures a fine grain-size and increases the mechanical strength by both solid solution and dispersoid strengthening. Another common alloying element is Cu that mainly contributes to strength by solid solution hardening and is also commonly used for precipitation hardening. All alloying elements influence other material properties such as proof stress and elongation as well [1]. AA3003 alloy is a widely used commercial aluminum alloy, containing manganese (Mn), iron (Fe), and silicon (Si) as alloying elements. According to Li et al., during solidification, constituent particles such as Al_6(Mn,Fe) and α-Al(Mn,Fe)Si form in the alloy, mainly as interdendritic eutectic networks [2]. α-Al(Mn,Fe)Si is the dominant dispersoid precipitated in commercial AA3xxx (Al–Mn–Fe–Si) alloys and some Mn-bearing 5xxx and 6xxx series alloys, which is mainly used for texture modification [3–5].

Aluminum alloys are commonly used for heat exchangers in the automotive industry due to an interesting combination of properties (low density, good thermal conductivity, satisfactory mechanical properties, and relatively good corrosion resistance). Unfortunately, cold-rolled Al alloy sheets are known to have a relatively poor formability compared with other conventional materials used in automotive applications, such as sheet steel [6].

More importantly, the recovery and recrystallization kinetics are significantly retarded by large amounts of Mn supersaturation in Al-Mn-based alloys, which is commonly referred to as concurrent precipitation [7,8]. Therefore, in order to suppress the concurrent precipitation, microstructure control by homogenization treatment prior to the cold-rolling and subsequent annealing is an important issue in advanced engineering processing in Al-Mn-based alloys [9,10].

During the production of materials for heat exchangers, the Al sheets are multi-layered, consisting of at least two Al alloy layers. The core layer is often a manganese (Mn)-rich AA3xxx series alloy, which provides strength to the assembly, while the clad layer is a silicon (Si)-rich AA4xxx series alloy. The high Si content of the clad alloy sufficiently depresses the melting temperature such that, during brazing, the clad alloy is either partially or fully liquid, while the core alloy remains solid. The AA4045 alloy forms a eutectic during brazing. The brazing material is used to form heat exchangers and radiators, thus the sheets also need to be corrosion resistant. There are various methods used for cladding in the aluminum industry, e.g., strip cladding, roll-bonding, or welding, and in this study roll-bonding was applied.

In order to fully exploit the dispersoid Al_6(Mn,Fe) hardening effect, a more systematic study on the influence of soaking or holding time on the precipitation behavior has been conducted. The objective of the current study was to determine the effects of isothermal holding time on the microstructure and mechanical properties, especially the hardness of AA3003 cladded with AA4045 alloy for heat exchangers' application.

2. Materials and Methods

2.1. Materials Preparation

The as-received AA4045 and AA3003 aluminum material (in homogenized condition) were in the form of plates with dimensions of 200 mm (length) × 160 mm (width) × 30 mm (thickness). These plates were then sectioned into a thickness ratio of 1:10 (3 mm:30 mm). The two-layer Al composite plates with dimensions of 110 mm (length) × 55 mm (width) × 30 mm (thickness) for AA3003, and 110 mm (length) × 55 mm (width) × 3 mm (thickness) for AA4045 are shown in Figure 1. This set-up was used as the starting pack material in the present investigation. The chemical compositions of the AA3003 and AA4045 alloys are given in Table 1. Spark emission spectrometry was used to determine the chemical composition.

Figure 1. The two-layer Al composite plates (pack) prepared for hot roll-bonding.

Table 1. Chemical compositions of the modified AA3003 core and AA4045 Al clad material (wt.%).

Material	Elements wt.%						
	Si	**Fe**	**Cu**	**Mn**	**Mg**	**Cr**	**Al**
AA3003	0.06	0.20	0.42	1.50	0.21	0.01	Bal
AA4045	10.10	0.15	-	0.02	0.01	-	Bal

2.2. Experimental Procedure

The AA3003 and AA4045 alloys used in the present work went through a number of processing stages, namely the preparation of stack (sandwich or pack), reheating (soaking), hot roll-bonding, annealing, cold-rolling, and annealing, as illustrated in Figure 2 [11]. The packs of AA4045/AA3003 were heated from room temperature at a heating rate of 60 °C/h up to the soaking temperature of 505 °C (±5 °C). Two sets of stacks were held for six different times, i.e., 20, 30, 35, 38, 40 and 45 h at this temperature, and the first stack was removed and air cooled, whilst the second pack was hot roll-bonded by rolling from 33 mm to 10 mm thickness under no lubrication in multiple passes. For hot-rolling (HR), the stacks were first heated to the rolling temperature of 505 °C in the air-circulated furnace and put back into it after each rolling step for about 10 min to avoid critical losses in temperature. These tests were carried out to simulate the extended times that the ingots spend in the preheated furnaces due to equipment breakdown [12]. A further reduction in thickness was carried out through cold-rolling (at room temperature) after intermediate annealing from 10 mm to a 0.3 mm final gauge. Cold-rolling was performed in the direction parallel to the hot-rolling direction as illustrated in Figure 2. The cold roll-bonded sheets (S-CR) were then annealed at 330 °C for 3 h in the air-circulated furnace (S-CRA).

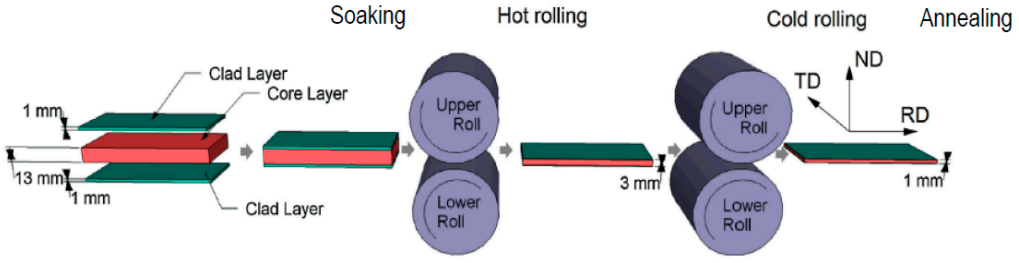

Figure 2. Schematic illustration of the clad sheet processing by hot roll-bonding [11].

This study focuses on the pre-brazed material (after annealing but before brazing) shown on the left in Figure 3. This schematic presentation illustrates the disappearance

of the interface after brazing. This interface is the core-cladding interface. The materials employed for heat exchangers are brazed, and this study focuses on aspects which occur before brazing the materials [13].

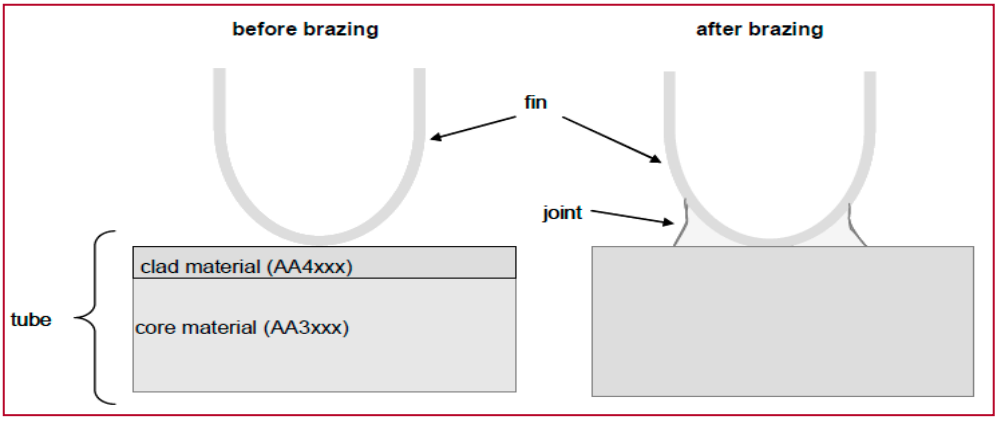

Figure 3. Schematic brazing process for heat exchangers [13].

2.3. Test Method

Small samples of 15 mm × 10 mm in size were cut from the as-received plates and the roll-bonded AA4045/AA3003 sheets for materials characterization. The samples were ground using SiC papers with a successively fine particle size to reduce the surface roughness. Final polishing was conducted using a velvet cloth and a diamond suspension polishing solution (0.1 µm particle size). The as-received plates and roll-bonded samples were then etched with Kroll's reagent (92 mL distilled water, 6 mL nitric acid, and 2 mL hydrofluoric acid) to reveal the second phase particles [11].

Bright field (BF) light optical microscopy (LOM) was conducted on a plane perpendicular to the transverse direction (TD). In order to observe the grain structure using polarized light optical microscopy (PLOM), samples were anodized with Barker's reagent (a mixture of 20% fluoroboric acid and 80% distilled water) [8]. For BF-LOM and PLOM, an Olympus DSX510 (Olympus, Center Valley, PA, USA) high-resolution upright motorized microscope with 13× zoom optics equipped with Olympus software version 3.1.1 was used. The analyses were performed on cross-sections of the as-received samples.

For electron backscattered diffraction (EBSD), the samples were electropolished with Struers A2 solution, a mixture of methanol and perchloric acid (80:20 ratio), at −10 °C and 35 V for 15 s after diamond polishing on a Struers LectroPol-5 machine. This was performed in order to remove the damage on the surface caused by grinding and mechanical polishing. A Jeol (Jeol, Akishima, Japan) scanning electron microscope (SEM) equipped with Aztec software version 4.1 for processing with a step size of 5 microns was used to obtain the EBSD data. The Oxford Instruments (Abingdon, UK) HKL Channel5 software version 5.1. was used for the post-processing of the EBSD data and measuring of the grain size. All the data points with a confidence index (CI, which typically represents the accuracy of indexing during EBSD data acquisition) of less than 0.1 were removed during post-processing [14]. The grain size was measured for the as-received material and for six reheated treatments at different times from the EBSD data of AA3003 alloy samples using the Oxford Instruments HKL Channel5 software version 5.1. Four grain-size measurements per sample were performed and averaged.

For scanning electron microscopy (SEM), the samples were examined using a Zeiss Supra55 VP Field Emission Scanning Electron Microscope (Zeiss, Oberkochen, Germany) equipped with an Oxford Inca microanalysis system with an accelerating voltage of 20 kV. Semi-quantitative energy dispersive spectrometer (EDS) microanalysis (Oxford Instruments, Abingdon, UK) was also performed, and EDS measurements were mainly made in spot mode to characterize the composition of individual phases. However, scanning mode was also used to estimate the nominal composition of the alloys by counting over appropriate

"windows": 200 µm × 200 µm in size in the case of the core material, and 10 µm × 200 µm for the cladding.

The macro-hardness using a DuraVision EmcoTest (EmcoTest, Kuchl, Austria) with a load of 5 kg was used to measure the hardness of the 33 mm thick AA3003 as-received and after six reheated treatment at different time samples, i.e., 20, 30, 35, 38, 40, and 45 h (not roll-bonded (NR)). These samples were roll-bonded down to 10 mm thick, inter-annealed, further cold-rolled (CR) to 0.3 mm thick sheets, and annealed (CRA). The micro-hardness using an InnovaTest Falcon 400 (InnovaTest, Maastricht, The Netherlands) with a load of 2 kg was used to measure the hardness of these cold-rolled and annealed (CRA) 0.3 mm thick sheets.

3. Results and Discussion

3.1. Microstructure—As-Received and Not Roll-Bonded

In the DC-cast 3003 material, the aluminum (Al) matrix is supersaturated with manganese (Mn) and silicon (Si) [15]. Therefore, a homogenization heat treatment before mechanical processing is essential to eliminate micro-segregation, reduce solid solution level of Mn, and obtain the right size and density of constituent particles and fine dispersoids [16]. The materials used in this study were received in the homogenized state. Figure 4a shows the microstructure of the as-received sample in an as-polished condition (unetched) that was composed of Mn-containing intermetallic particles (constituent particles) shown by red arrows in the aluminum matrix. Figure 4b shows the microstructure of the as-received sample in the etched condition that was composed of α-Al dendrites, shown by yellow arrows and a number of Mn-containing intermetallic particles shown by red arrows [16], which were distributed on grain boundaries. It is known that for 3xxx alloys with coarse dendrite arms, the distribution of dispersoids is rather inhomogeneous, having a much lower density in the center region of dendrite arms due to the segregation of Mn [16].

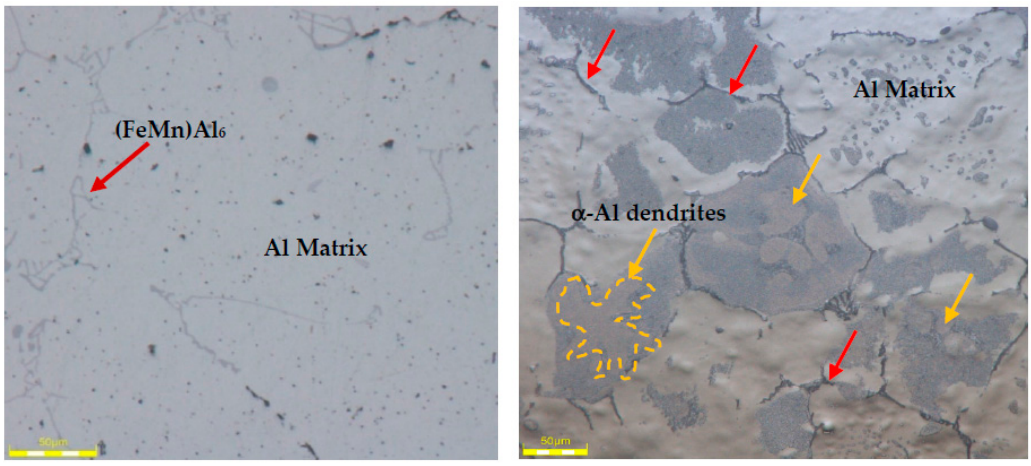

(**a**) (**b**)

Figure 4. Optical micrographs of the AA3003 alloy in its as-received condition, showing the morphology and certain characteristic sizes of: (**a**) the as-polished condition showing primary particles (red arrows); (**b**) etched conditions showing the dendritic arm structure in yellow arrows, while the red arrows show primary particles/constituents on grain boundaries.

Figure 5a–e show the electron backscattered diffraction (EBSD) maps showing the microstructure of the AA-3003. Initially, the as-received alloy had large grain structure with average grain size approximately 90.8 µm. When the alloy is reheated for longer periods, the grain size decreases slightly. It can be seen that after holding for 38 h, the average grain size of the AA3003 alloy decreased from 90.8 to 77.1 µm. By reheating for longer periods, it slightly increases up to 86.9 µm which indicates that coarsening is the main mechanism to

control the evolution of the microstructure. The quantitative values of average grain size of as-received and non-roll-bonded samples are listed in Table 2. One can also see that the grains are smaller at 38 h than that of the as-received material (see Figure 5e).

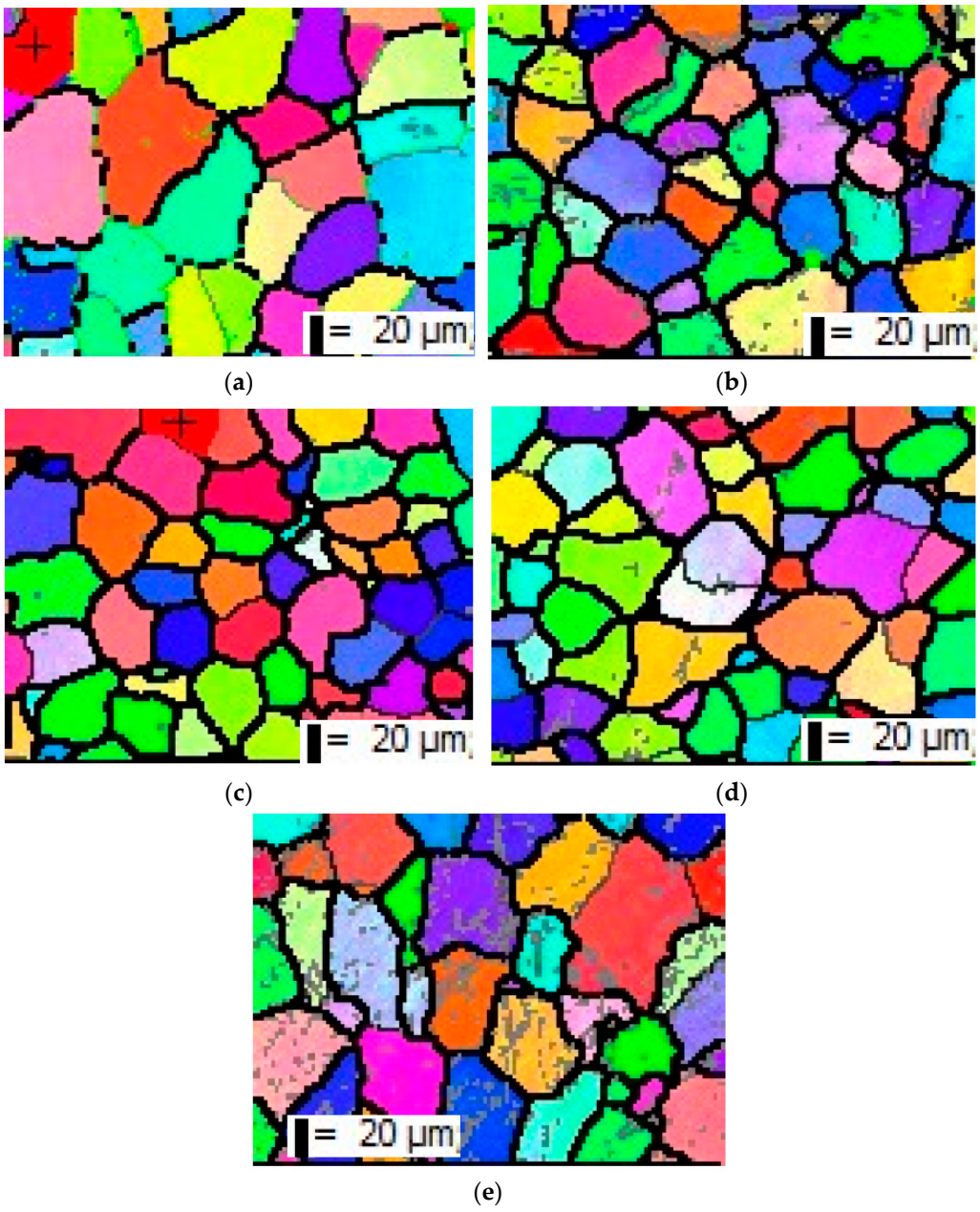

Figure 5. Electron backscattered diffraction (EBSD) maps showing the microstructure of the modified AA3003: (**a**) as-received (homogenized), d_{Av} 90.8 µm; (**b**) 35 h at 505 °C, d_{Av} 88.4 µm; (**c**) 38 h at 505 °C, d_{Av} 77.1 µm; (**d**) 40 h at 505 °C, d_{Av} 83.8 µm; (**e**) 45 h at 505 °C, d_{Av} 86.9 µm.

Table 2. Change in grain size in the AA3003 aluminum alloy by soaking at 505 °C for different times.

Condition	Average Grain Size (µm)	Stdev
As-received	90.82	8.12
35 h	88.44	13.27
38 h	77.11	7.66
40 h	83.79	5.72
45 h	86.91	4.63

Figure 6 shows the SEM micrographs of the AA3003 alloy reheated to 505 °C, and held for 20, 30, 38, and 40 h, showing the formation of precipitates (dispersoids) and the evolution of the morphology of the primary or constituent particles, shown in red arrows. When the alloy is reheated for longer periods, the size of the primary particles slightly increases, which indicates that coarsening is the main mechanism to control the evolution of the primary particles. The dispersoid phase competes with constituent particles for the solute and this can lead to the dissolution of dispersoids in the regions adjacent to large constituents on prolonged heating (as part of this study), leading to dispersoid-free zones adjacent to coarse constituent particles. A large quantity of rod-like, plate-like, and network eutectic primary particles are distributed in the interdendritic regions and grain boundaries. A slow increase in the average thickness of particles can also be observed, especially for those held at ≥38 h.

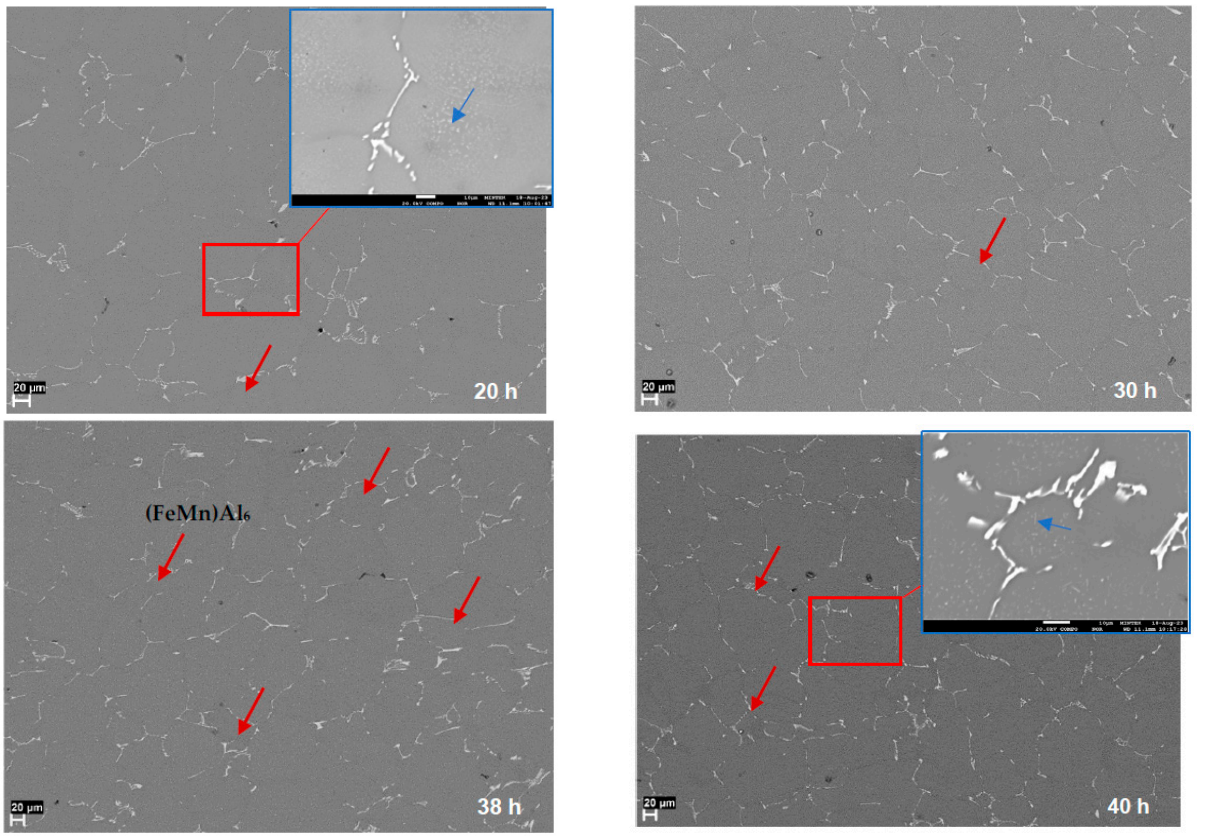

(**a**) (**b**)

Elements	20 hr	40 hr
Al	91.59	95.48
Si	2.58	0.26
Mn	4.71	2.77
Fe	0.13	0.1
Cu	0.49	1.49

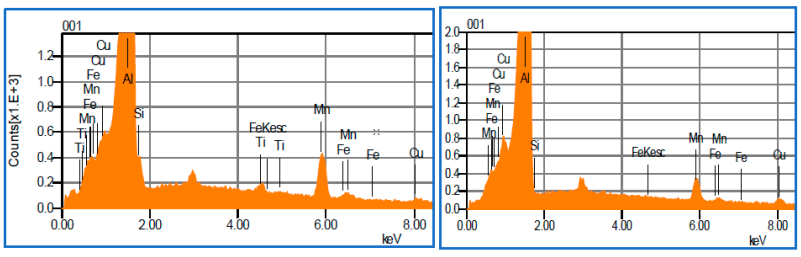

(**c**) di dii

(**d**)

Figure 6. (**a**,**b**) SEM-BSE images of the AA3003 alloy reheated and held for 20, 30, 38, and 40 h, showing the evolution of the morphology of the primary particles (shown in red arrows). The precipitates are shown in the insert, which is approximately taken from the position indicated by the square frame. (**c**) the compositions (mass %) of the precipitates were identified and (**d**) the EDS spectra of the precipitates after, (**di**) 20 h and (**dii**) 40 h.

The 40 h micrograph is insightful because it agrees with the hardness peak that is discussed in Section 3.3 of this paper. This is attributed to the emergence of fine precipitates in the matrix as shown in the insert, which is approximately taken from the position indicated by the square frame (Figure 6). There is a coarsening of the grain boundary precipitates at 40 h, which would lead to a lower hardness value, but it is superseded by the strengthening effect of the emerging precipitates in the matrix. When the alloy is re-heated from room temperature to a temperature of 505 °C, there is nearly no change in the morphology and grain size of primary particles. The eutectic networks of primary particles begin to break up after soaking for 40 h. The presence of rectangular-shaped precipitates was also identified, with the help of EDX analyses, as Al-Mn: see the insert of Figure 6b.

Scanning electron microscopy (SEM) was undertaken to analyze the chemical composition and the phase in the investigated alloys. Figures 7–9 show the SEM micrographs and the EDS maps for different elements observed in the alloys. The EDS maps confirm the uniform distribution of the constituent phases along the dendritic arms.

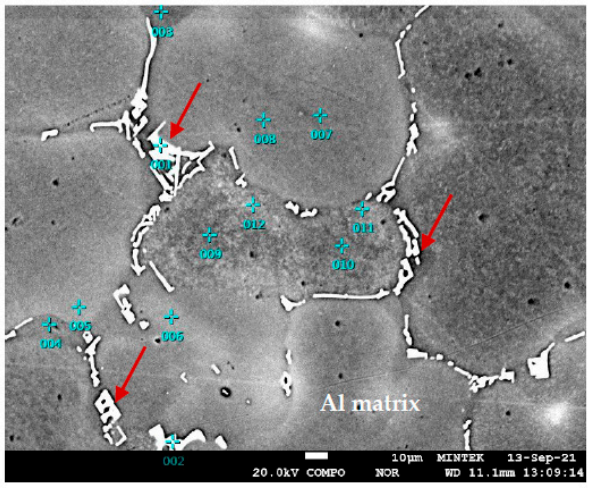

(**a**)

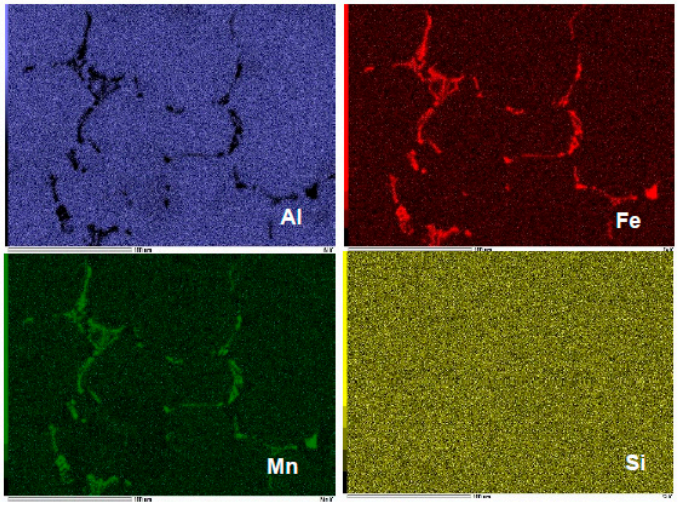

(**b**)

Spot	Fe	Al	Mn	Total
1	7.2	82.7	10.1	100.0
2	12.2	71.3	16.5	100.0
3/4/7/8	-	100.0	-	100.0
9/10/11/12	-	100.0	-	100.0
5/6		97.9	2.1	100.0

(**c**)

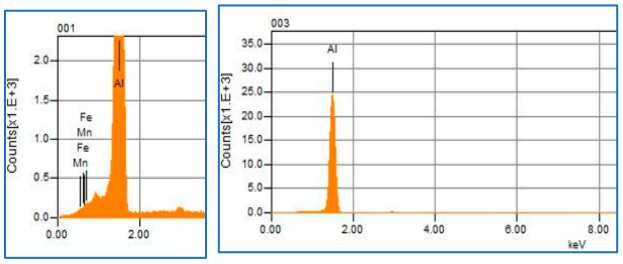

di dii

(**d**)

Figure 7. (**a**) SEM-BSE image of the as-received AA3003 alloy, (**b**) elemental maps by SEM-EDS showing: aluminum; iron, manganese, and silicon maps, respectively, (**c**) the compositions (wt.%) of the constituent particles were identified, and (**d**) the EDS spectra of the constituent (**di**) and the Al matrix (**dii**).

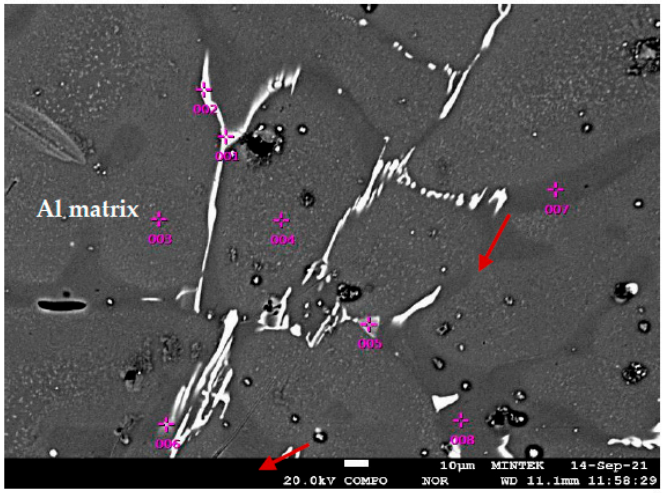

(**a**)

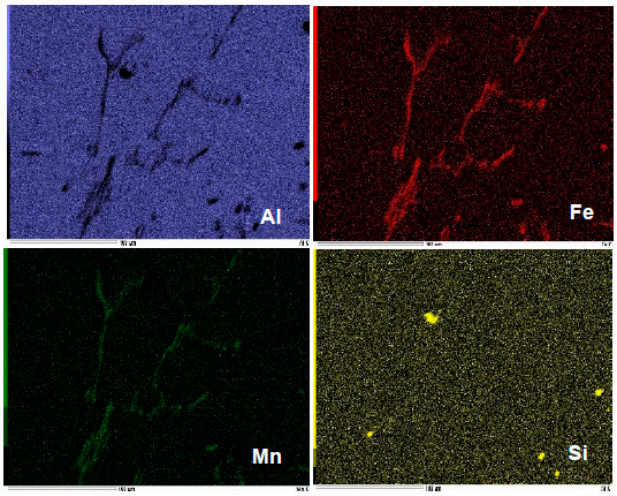

(**b**)

Spot	Fe	Al	Mn	Total
1/2	13.24	69.55	17.21	100
3/4/7/8	-	100	-	100
5	-	91.32	8.68	100
6	7.98	79.74	12.27	99.99

(**c**)

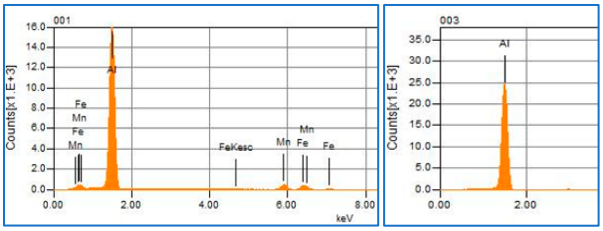

di dii

(**d**)

Figure 8. (**a**) SEM-BSE image of the reheated material and that held for 20 h for the AA3003 alloy, (**b**) elemental maps by SEM-EDS showing: aluminum; iron, manganese, and silicon maps, respectively, (**c**) the compositions (wt.%) of the constituent particles were identified, and (**d**) the EDS spectra of the constituent (**di**) and the Al matrix (**dii**).

Figure 7 presents the morphology of the Fe, Mn-rich constituent particles in the as-cast AA3003 alloy characterized by SEM with corresponding EDS elemental mapping results. As can be seen in Figure 7, the constituent particles of the skeletal shape are distributed mainly in the inter-dendritic regions, and most of them have been identified as the Al_6(Mn,Fe) phase by EDS and were formed during solidification. These intermetallic particles were also found to contain Fe, Mn, and Si (Figure 8). The resolution of EDS is in the range of some μm, so the aluminum matrix also influences the EDS. EDS results showing an estimation of the measurement error are summarized in Table 3. Both the iron and manganese content of the Al_6(Mn,Fe) phase seemed to be stable as the soaking time increased, indicating that the latter did not attain an equilibrium state during the DC casting process. The Al-matrix also does not change in chemical composition. This is evidence that it is not only the formation of fine precipitates from supersaturation at extended soaking times, but that further transformation of the Al_6(Mn,Fe) phase took place. According to Hamerton et al. [17], Al_6(Fe,Mn) has an acicular shape in the as-cast sample; and after long heat treatment, they become coarser. It must be noted that EDS alone is not sufficient for phase analysis and transmission electron microscopy (TEM) is planned to be conducted.

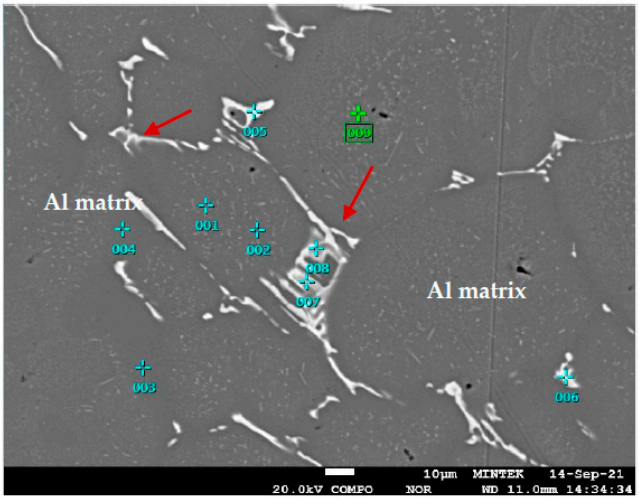

(**a**)

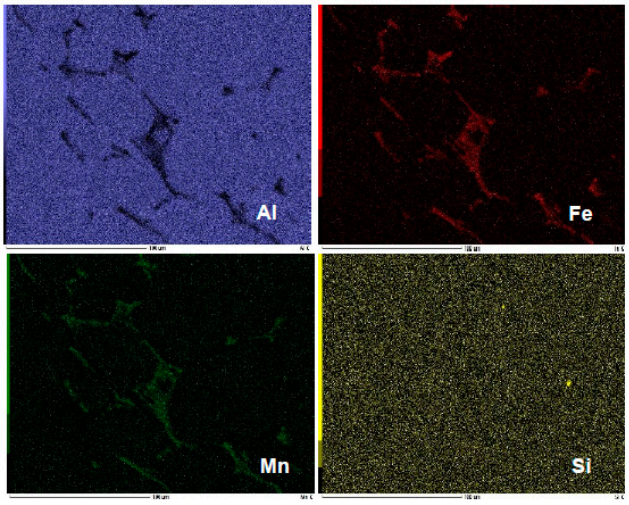

(**b**)

Spot	Fe	Al	Mn	Total
1	-	97.6	2.4	100
7	-	88.82	11.18	100
2/3/4	-	100	-	100
5/6/8	17.2	66.31	16.5	100

(**c**)

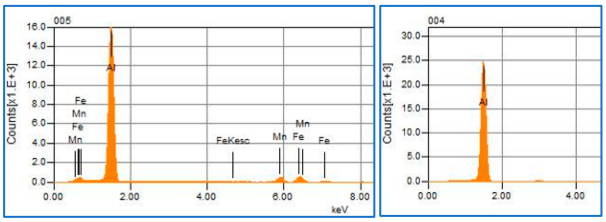

di dii

(**d**)

Figure 9. (**a**) SEM-BSE image of the reheated material and that held for 45 h for the AA3003 alloy, (**b**) elemental maps by SEM-EDS showing: aluminum; iron, manganese, and silicon maps, respectively, (**c**) the compositions (wt.%) of the constituent particles were identified, and (**d**) the EDS spectra of the constituent (**di**) and the Al matrix (**dii**).

Table 3. The SEM-EDS results of the intermetallic particles found in the AA3003 aluminum alloy soaked at 505 °C for different times.

Condition	Fe (wt.%)	Mn (wt.%)
As-received	9.69 ± 3.57	13.32 ± 4.54
20 h	12.44 ± 4.12	15.94 ± 3.23
30 h	10.45 ± 2.65	13.91 ± 2.50
38 h	13.05 ± 4.39	14.92 ± 4.21
40 h	12.51 ± 2.10	14.17 ± 3.05
45 h	9.80 ± 6.67	11.54 ± 5.57

3.2. Roll-Bonding Interface Microstructure

Figure 10 shows the typical microstructures at the interfaces of all samples before (sandwich) roll-bonding and after holding at 505 °C for 45 h and hot roll-bonding. It is evident that a complete metallurgical fusion was achieved. In other words, micro or macro defects are not observed in the inter-layer boundaries, which confirms successful bonding of the layers by hot roll-bonding. According to the literature [18–20], the roll-bonding process, among solid-state joining processes, has shown significant potential and can be classified among the solid-state processes in which extensive mechanical deformation is produced in a metallic sheet with or without the application of heat to change the microstructure or to create bonds between multiple metal sheets. Subsequent annealing stimulates the diffusion between the layers, which on the one hand leads to a better bond strength, but on the other hand leads to the formation of intermetallic phases on the interface, which in turn can have different effects depending on the metals and alloys used as composite components [21–25].

Alexander et al. [26], studied the transformation of intermetallic particles from $Al_6(Fe, Mn)$ to α-Al–(Fe, Mn)–Si that occurs upon homogenization of 3xxx aluminum alloys and found that this occurs by diffusing silicon into an Al–Fe–Mn alloy. According to the literature, the fraction of α-Al(MnFe)Si particles transformed from Al_6(Mn,Fe) increases with the heating temperature and homogenization time. In this current study, the heating temperature was kept constant and the soaking time was varied. This study was on the effect of the soaking time on the properties of the modified AA3003. Also, the degree of transformation of the Al_6(Fe,Mn) phase to α-Al-(Fe,Mn)-Si phase is important for subsequent processing such as rolling into sheets. This transformation requires the diffusion of silicon from the matrix to the particle. It was found that significant dispersion strengthening by α-Al(Mn,Fe)Si dispersoids at room and elevated temperatures can be achieved in 3xxx aluminum alloys via appropriate heat treatments or the modification of alloy compositions.

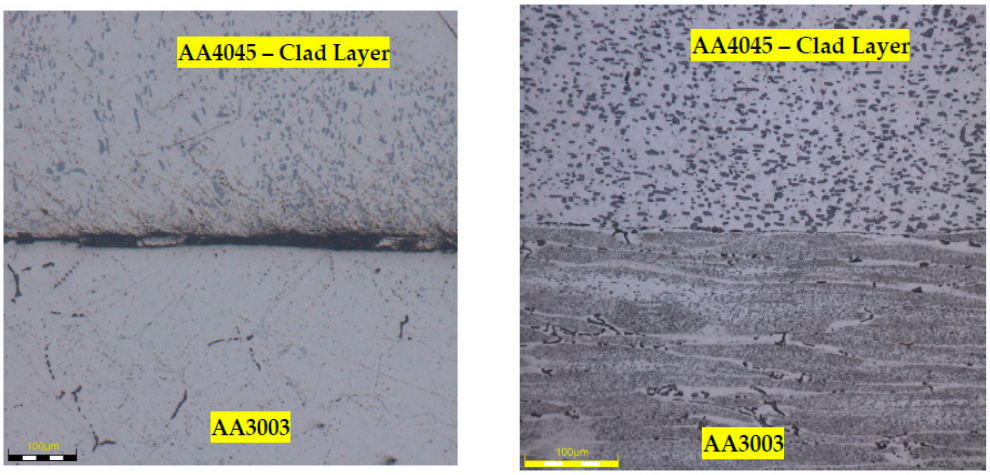

(**a**) (**b**)

Figure 10. Optical micrographs of AA4045/AA3003 showing (**a**) sandwich samples before roll-bonding and (**b**) after a 60% reduction showing a good bonding interface.

Figure 11a shows the SEM images of the Al cladding alloys after sheet processing to 0.3 mm including annealing (i.e., soaking for 20 h at 505 °C, cold-rolled and annealed at 330 °C for 3 h (S-CRA)) indicating Si particles distributed in the clad layer (red arrows). Due to the high roll-bonding temperature, the interface is almost invisible; resulting in a complete metallurgical fusion, shown by a yellow line and arrows showing particles in the core. The thickness of the cladding layers was about 90 to 100 µm. The manganese map by SEM-EDS in Figure 11b shows a distinct interface between the substrate AA3003 and the cladding AA4045. The reheating and subsequent hot- and cold-rolling led to the break-down, spheroidization, and uniform distribution of the eutectic Mn-Fe particles of AA3003. As expected, the microstructure is inhomogeneous and reveals various precipitates and particles such as Al–Fe–Mn–Si block-like and α-Al(Fe,Mn)Si precipitates shown by yellow arrows. This shows α-Al, Si and AlFeSi phases on the AA4343 clad material side, and α-Al, Al_6Mn, and AlFeMnSi phases on the AA3003 core material side. In the literature [27,28], the roll-bonding process has a significant grain refinement effect on aluminum alloys, and the process parameters must play an important role in the microstructure of the final products. Therefore, further studies need to be conducted to optimize the roll-bonding process. The effects of process parameters such as the rolling speed and temperature on microstructures should particularly be focused on. After hot- and cold-rolling of the as-received material, large particles of intermetallic (mainly in the form of Chinese script morphology consisting of Fe-Mn-Si) were broken into smaller particles with an increased Fe, Mn, and Si content, indicating the formation of an α-Al(Fe,Mn)Si phase [29] as compared to before rolling.

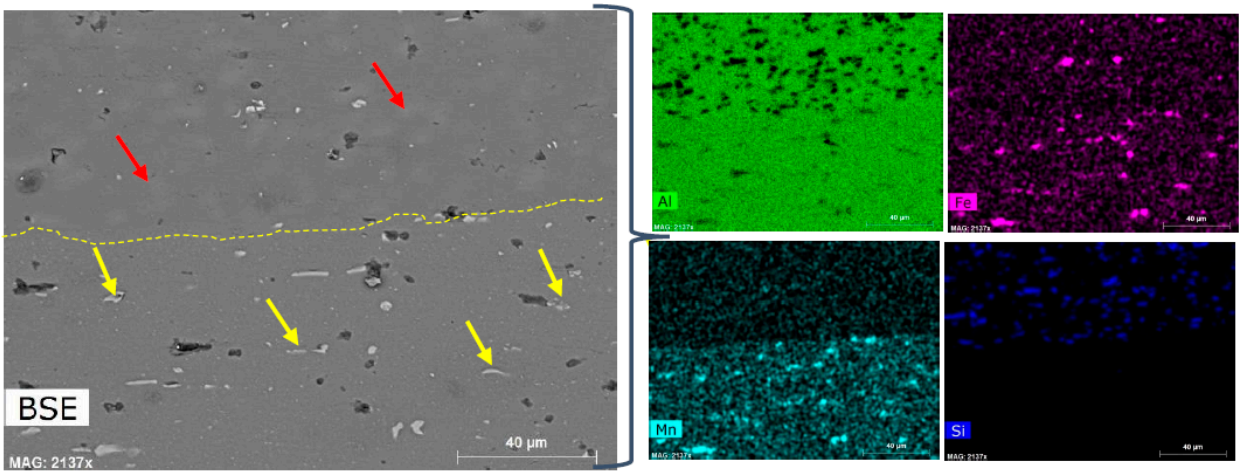

(**a**) (**b**)

Figure 11. (**a**) SEM-BSE image of AA3003 after soaking for 20 h at 505 °C, cold-rolled to 0.3 mm thick sheets, and annealed at 330 °C for 3 h (S-CRA), showing a good bonding interface, (**b**) elemental maps by SEM-EDS showing: aluminum; iron, manganese, and silicon maps, respectively.

According to Pokov et al. 2011, [30], eutectic colonies of primary particles break up at temperatures above 560 °C. Also, during the thermomechanical treatment, the precipitation of dispersoids and coarsening of primary phases occur. During annealing, Al6(Fe,Mn) transforms into an α-phase owing to the diffusion of silicon from the solid solution. The decrease in the Fe:Mn ratio during the transformation implies that the diffusion of Mn is of importance too. The α-phase nucleates at the Al6(Fe,Mn)-matrix interface and propagates into Al6(Fe,Mn) as an eutectoid reaction front. It must be noted that iron and manganese can substitute for each other in the Al(Fe,Mn)Si and orthorhombic Al6(Fe,Mn) phase [30].

3.3. Vickers Hardness

Figure 12 shows the Vickers hardness (HV) measurements for the as-received, soaked at 505 °C for six different times (not rolled), soaked and cold-rolled (S-CR), and soaked, cold-rolled, and annealed (S-CRA) samples. As may be seen, the hardness of the as-received material remains constant with the increase in the soaking time. The hardness showed a slight increase of about ±10 HV after 40 h, indicating that there was still some supersaturation of Mn and copper (Cu) after the DC casting process (shown by a horizontal line, Line 1). The Al–Mn alloys cannot be strengthened by heat treatments but can be strengthened in the way of micro-alloying. In this case, the alloy studied was micro-alloyed with copper (Cu) of 0.42 wt.% as compared to the commercial AA3003. The addition of copper tends to reduce the solid solubility of Mn in the matrix of AA3003-0.4%Cu and thus promotes the precipitation of α-Al(Mn,Fe)Si dispersoids. Therefore, as expected, we could see some precipitates in the matrix of the preheated AA3003 that led to a gradual change in hardness.

The hardness of all of the S-CRA samples (90% thickness reduction) were the same within error bars, i.e., with a slightly high hardness at 35 and 40 h (shown by a horizontal line, Line 2). Line 3 shows that there was an improvement in the hardness of S-CR for all soaking times, possibly due to the cold-rolling (strain hardening) effect. The increase in hardness, as the result of cold work, is due to the strain-hardening mechanism of this alloy. Cold-rolling induces dislocations, contributing to increased hardness. Cold-rolling achieves very high strains, which can be as high as six to seven in thin gauge foil rolling, and the strength attained relies on maintaining a level of work hardening even at high strains [31]. The formed dispersoids provide a significant direct strengthening effect and influence the work-hardening behavior of the material.

The subsequent decrease in hardness after annealing (Line 2) for the S-CRA samples is due to recovery effects, which involve annihilation point defects and dislocations. Although the annealing may not have initiated complete recrystallization after cold-rolling, the hardness did not return to the as-received (homogenized) level.

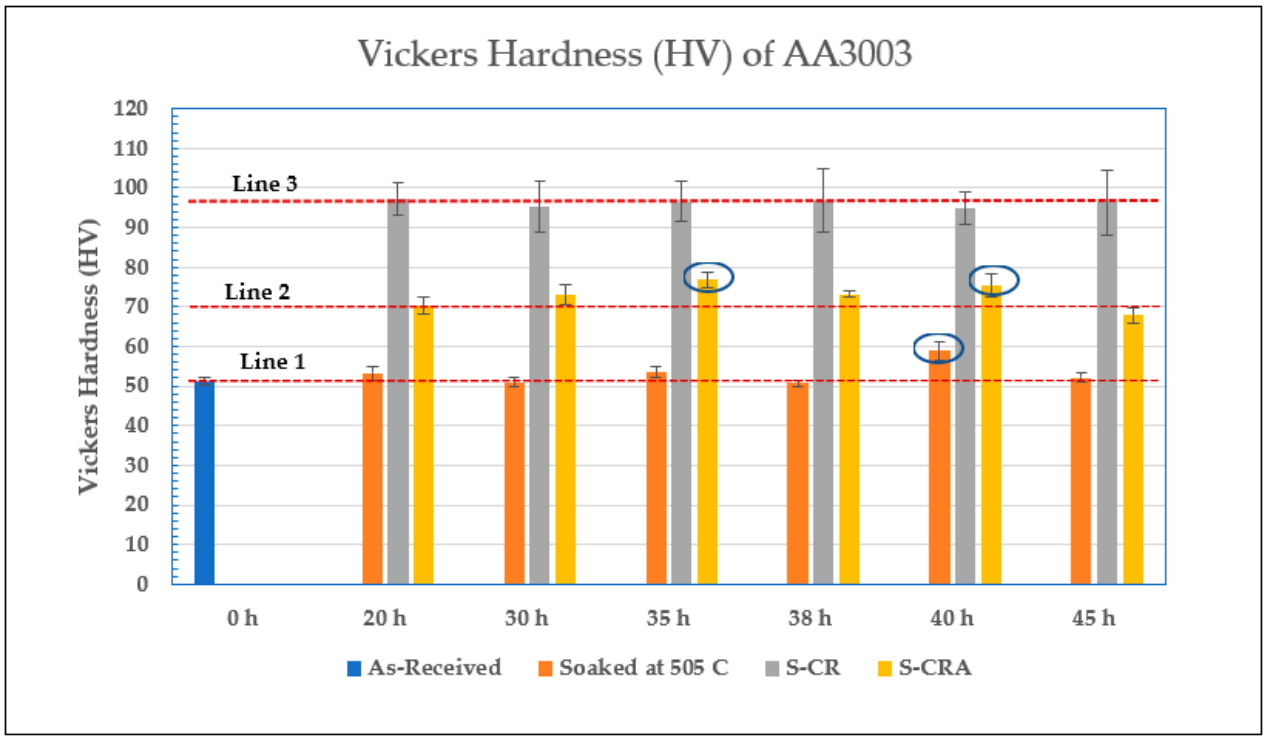

Figure 12. Vickers hardness (HV) measurements of the samples as-received, soaked at 505 °C, soaked and cold-rolled (S-CR), and soaked, cold-rolled, and annealed at 330 °C for 3 h (S-CRA).

Initially, the as-received alloy had a large grain structure with an average grain size of approximately 91 µm. After hot-rolling bonding and subsequent cold-rolling, microstructure showed a banded structure due to a higher dislocation density. After annealing, a fine, uniform, and nearly equiaxed structure was obtained. It is expected that the fine and uniform grain structure in the annealed material will result in increased hardness compared to the as-received material [32]. Additionally, other researchers have indicated that grain refinement has been recognized as an efficient way to improve the mechanical properties of aluminum alloys [33]. Specifically, grain refinement can significantly enhance the hardness, strength, and plasticity of aluminum alloys [34].

Coarsening of the α-Al(Mn,Fe)Si dispersoids was only observed after soaking for 45 h and these coarse precipitates contributed to the lower hardness after cold work and annealing at 330 °C for 3 h (Figure 5). Long residence times during the preheat stage resulted in Mn-bearing dispersoids coarsening and this in turn resulted in early recrystallisation during temper annealing and thus a lower hardness.

4. Conclusions

The microstructures, surface structure, and mechanical properties at room temperature of the AA3003 cladded with Al–Si system (AA4045) alloy have been investigated. The main conclusions can be summarized as follows:

- The laboratory hot roll-bonding process for the production of the AA3003/4045 aluminum sheets has been successfully developed (Off-line TMP), i.e., complete bonding was achieved in the interface after roll-bonding.

- The as-received microstructure for AA3003 showed a coarse grain structure, and decreased after soaking for 38 h; however, a slight increase in grain size was shown at the 45 h soaking period.
- Coarsening of the α-Al(Mn,Fe)Si dispersoids at 505 °C was only observed at 45 h soaking time, which was, as expected, accompanied by a slight decline in hardness.
- The α-Al(Mn,Fe)Si was found to be the dominant dispersoid precipitate in the modified AA3003 core.
- The hardness trend with soaking time was found to be similar to that after soaking, cold working, and annealing, with an increase in hardness in the latter possibly due to strain hardening (from cold-rolling).
- Longer residence times in the preheat furnace coarsen Mn-bearing dispersoids. This results in early recrystallisation and a slightly lower hardness.

Author Contributions: J.S.M.: Conceptualization, data curation, writing—original draft preparation, review and editing. C.W.S.: Supervision, formal analysis, review and editing, final approval of the version to be published. V.K.M.: Interpretation of data for the work, writing—review and editing. T.B.: Data validation, review and editing. All authors have read and agreed to the published version of the manuscript.

Funding: The Department of Science and Innovation (DSI)—Advanced Materials Initiative (AMI), through the Ferrous Materials Development Network (FMDN), financially supported this work, in addition to the Department of Minerals, Resources, and Energy (DMRE) through State Grant and Mintek.

Data Availability Statement: Not applicable.

Acknowledgments: The authors would like to thank Mintek South Africa for financial support and Hulamin for supplying materials, as well as Mbavhalelo Maumela and Eddie Innes for their involvement during the roll-bonding process.

Conflicts of Interest: The author declare no conflict of interest.

References

1. Hirsch, J. (Ed.) *Virtual Fabrication of Aluminum Products*; WILEY-VCH: Weinheim, Germany, 2006; pp. 19–26.
2. Backerud, L.; Krol, E.; Tamminen, J. *Solidification Characteristics of Aluminium Alloys: Wrought Alloys*; Skanaluminium, Universitetsforlaget AS: Oslo, Norway, 1986; Volume 1, pp. 93–97.
3. Li, Y.J.; Arnberg, L. Quantitative study on the precipitation behavior of dispersoids in DC-cast AA3003 alloy during heating and homogenization. *Acta Mater.* **2003**, *51*, 3415–3428. [CrossRef]
4. Li, Y.J.; Muggerud, A.M.F.; Olsen, A.; Furu, T. Precipitation of partially coherent α-Al (Mn,Fe)Si dispersoids and their strengthening effect in AA 3003 alloy. *Acta Mater.* **2012**, *60*, 1004–1014. [CrossRef]
5. Li, Y.J.; Zhang, W.Z.; Marthinsen, K. Precipitation crystallography of plate-shaped Al 6(Mn,Fe) dispersoids in AA5182 alloy. *Acta Mater.* **2012**, *60*, 5963–5974. [CrossRef]
6. Bolt, P.J.; Lamboo, N.A.; Rozier, P.J. Feasibility of warm drawing of aluminium products. *J. Mater. Process. Technol.* **2001**, *115*, 118–121. [CrossRef]
7. Pimenta, F.C., Jr.; Arruda, A.C.; Padilha, A.F. Resistance to recrystallization in Al-1% Mn alloys. *Z. Für Met.* **1986**, *77*, 522–528.
8. Nagahama, K.; Miki, I. Precipitation during recrystallization in Al-Mn and Al-Cr alloys. *Trans. Jpn. Inst. Met.* **1974**, *15*, 185–192. [CrossRef]
9. Sun, N.; Patterson, B.R.; Suni, J.P.; Simielli, E.A.; Weiland, H.; Allard, L.F. Microstructural evolution in twin roll cast AA3105 during homogenization. *Mater. Sci. Eng. A* **2006**, *416*, 232–239. [CrossRef]
10. Sun, N.; Patterson, B.R.; Suni, J.P.; Doherty, R.D.; Weiland, H.; Kadolkar, P.; Blue, C.A.; Thompson, G.B. Effect of Heating Rate on Recrystallization of Twin Roll Cast Aluminum. *Met. Mater. Trans. A* **2008**, *39*, 165–170. [CrossRef]
11. Mikhaylovskaya, A.V.; Mochugovskiy, A.G.; Kotov, A.D.; Yakovtseva, O.A.; Gorshenkov, M.V.; Portnoy, V.K. Superplasticity of clad aluminium alloy. *J. Mater. Process. Technol.* **2017**, *243*, 355–364. [CrossRef]
12. Buthelezi, T. *Review—Low Mechanical Properties on 9031 Clad Tubestock*; Confidential Technical Report; 2015.
13. Schäuble, K. Silica Passivation Layer on Aluminium Brazing Sheets. Ph.D. Thesis, Universität zu Köln, Köln, Germany, 2010.
14. *OIM*, Analysis Version 7.2. User Manual. TexSEM Laboratories Inc.: Draper, UT, USA, 2013.
15. Da Silva Junior, M.E.; Da Silva, C.V.; Araújo, H.R.; De Araújo, R.R.L.; Yadava, Y.P.; De Araujo Filho, O.O. Manufacturing and characterization of AA3003 aluminum alloy Powders by synthesis of elementary powders by techniques of High energy ball milling. *Int. J. Dev. Res.* **2022**, *12*, 58757–58761. [CrossRef]

16. Pan, S.; Qian, F.; Li, C.; Wang, Z.; Li, Y. Synergistic strengthening by nano-sized α-Al(Mn,Fe)Si and Al3Zr dispersoids in a heat-resistant Al–Mn–Fe–Si–Zr alloy. *Mater. Sci. Eng. A* **2021**, *819*, 141460. [CrossRef]
17. Hamerton, R.G.; Cama, H.; Meredith, M.W. Development of the coarse intermetallic particle population in wrought aluminium alloys during ingot casting and thermomechanical processing. *Mater. Sci. Forum* **2000**, *331*, 143–154. [CrossRef]
18. Mansouri, H.; Eghbali, B.; Afrand, M. Producing multi-layer composite of stainless steel/aluminum/copper by accumulative roll bonding (ARB) process. *J. Manuf. Process.* **2019**, *46*, 298–303. [CrossRef]
19. Khan, H.A.; Asim, K.; Akram, F.; Hameed, A.; Khan, A.; Mansoor, B. Roll Bonding Processes: State-of-the-Art and Future Perspectives. *Metals* **2021**, *11*, 1344. [CrossRef]
20. Frolov, Y.; Haranich, Y.; Bobukh, O.; Remez, O.; Voswinkel, D.; Grydin, O. Deformation of expanded steel mesh inlay inside aluminum matrix during the roll bonding. *J. Manuf. Process.* **2020**, *58*, 857–867. [CrossRef]
21. Chen, G.; Li, J.; Yu, H.; Su, L.; Xu, G.; Pan, J.; You, T.; Zhang, G.; Sun, K.; He, L. Investigation on bonding strength of steeln aluminum clad sheet processed by horizontal twin-roll casting, annealing and cold rolling. *Mater. Des.* **2016**, *112*, 263–274. [CrossRef]
22. Akramifard, H.; Mirzadeh, H.; Parsa, M. Cladding of aluminum on AISI304L stainless steel by cold roll bonding: Mechanism, Microstructure, and Mechanical Properties. *Mater. Sci. Eng.* **2014**, *613*, 232–239. [CrossRef]
23. Akramifard, H.; Mirzadeh, H.; Parsa, M. The effect of annealing treatment on mechanical properties of aluminum clad steel sheet. *Mater. Sci. Eng.* **2014**, *613*, 232–239. [CrossRef]
24. Jamaati, R.; Toroghinejad, M. Investigation of the parameters of the cold roll bonding (CRB) process. *Mater. Sci. Eng.* **2010**, *527*, 2320–2326. [CrossRef]
25. Soltani, M.; Jamaati, R.; Toroghinejad, M. The influence of TiO_2 nano-particles on bond strength of cold roll bonded aluminum strips. *Mater. Sci. Eng.* **2012**, *550*, 367–374. [CrossRef]
26. Alexander, D.T.L.; Greer, A.L. Nucleation of the Al6(Fe, Mn)-to-α-Al–(Fe, Mn)–Si transformation in 3XXX aluminium alloys. I. Roll-bonded diffusion couples. *Philos. Mag.* **2004**, *84*, 3051–3070. [CrossRef]
27. Yu, C.Y.; Sun, P.L.; Kao, P.W.; Chang, C.P. Mechanical properties of submicron-grained aluminum. *Scr. Mater.* **2005**, *52*, 359–363. [CrossRef]
28. Wang, J.; Horita, Z.; Furukawa, M.; Nemoto, M.; Tsenev, N.K.; Valiev, R.Z.; Ma, Y.; Langdon, T.G. An investigation of ductility and microstructural evolution in an Al—3% Mg alloy with submicron grain. *J. Mater. Res.* **1993**, *8*, 2810–2818. [CrossRef]
29. Liu, Y.; Huang, G.; Sun, Y.; Zhang, L.; Huang, Z.; Wang, J.; Liu, C. Effect of Mn and Fe on the Formation of Fe- and Mn-Rich Intermetallics in Al-5Mg-Mn Alloys Solidified Under Near-Rapid Cooling. *Materials* **2016**, *9*, 88. [CrossRef] [PubMed]
30. Pokova, C.M.; Lacaze, J. Enhanced AW3003 Aluminum Alloys for Heat Exchangers. In *WDS'11 Proceedings of Contributed Papers, Part III, Proceedings of the 20th Annual Conference of Doctoral Students—WDS 2011, Prague, Czech Republic, 31 May–3 June 2011*; MatfyzPress: Prague, Czech Republic, 2011; pp. 141–146. ISBN 978-80-7378-186-6.
31. Liu, Q.; Huang, X.; Lloyd, D.J.; Hansen, N. Microstructure and strength of commercial purity aluminum (AA1200) cold rolled to large strains. *Acta Mater.* **2002**, *50*, 3789–3802. [CrossRef]
32. Kumar, R.; Gupta, A.; Dandekar, T.R.; Khatirkar, R.K. Microstructure and texture development in AA3003 aluminium alloy. *Mater. Today Commun.* **2020**, *24*, 100965. [CrossRef]
33. Estrin, Y.; Vinogradov, A. Extreme grain refinement by severe plastic deformation: A wealth of challenging science. *Acta Mater.* **2013**, *61*, 782–817. [CrossRef]
34. Zhao, Y.; Liao, X.; Jin, Z.; Valiev, R.; Zhu, Y. Microstructures and mechanical properties of ultrafine grained 7075 Al alloy processed by ECAP and their evolutions during annealing. *Acta Mater.* **2004**, *52*, 4589–4599. [CrossRef]